Experimental Assessment and CFD Simulations of Local Solid Concentration Profiles in a Pilot-Scale Stirred Tank*

M. ŠPIDLA**, M. MOŠTĚK, V. SINEVIČ, M. JAHODA, and V. MACHOŇ

Department of Chemical Engineering, Faculty of Chemical Engineering, Institute of Chemical Technology, CZ-166 28 Prague
e-mail: michal.spidla@vscht.cz

Received 1 April 2005

An experimental assessment of solid particle distribution in a stirred vessel was performed by conductivity measurements, and for the same solid-liquid system, the capabilities of the Computational Fluid Dynamics (CFD) simulation were investigated.

A detailed particle distribution measurement of a solid-liquid suspension at the just-suspended state was carried out in a pilot-plant stirred vessel of one meter in diameter. This baffled stirred tank was agitated with a pitched blade turbine, which generates an axial-flow pattern in the tank. The water suspension of glass beads of diameter 0.35 mm was studied. Average particle concentration was 5 vol. %. In this mode of experimental arrangement, a particle-filled layer of suspension was observed. Axial and radial particle concentration gradients and their standard deviations were determined.

CFD simulations were performed using a two-phase model implemented in the commercial code Fluent 6.2. The Eulerian-Eulerian multiphase model was adopted in conjunction with the Multiple Reference Frames and the "mixture" k-ε turbulence model.

Computational results are compared with the experimental data and critically discussed. The simulation results are in agreement with experiment, but the drag coefficient for particles settling in a stagnant fluid needs to be corrected in order to obtain acceptable results for a turbulent flow regime.

Turbulently agitated solid-liquid suspensions belong to common unit operations in technologies of chemical processes, biochemical industries, mineral processing industries, and many others. Mixing and dispersion of solids is involved in about 80 % of the operations. Relevant examples include crystallization, precipitation, leaching, dissolution, coagulations, and water treatment. Because of variety of applications, many different equipment configurations were studied, and especially for stirred tanks, the knowledge of local solid concentration distribution is very important.

At present, numerical approaches are developed to study many of the processes mentioned above. Computational Fluid Dynamics (CFD) becomes a powerful tool for predicting fluid flow, heat/mass transfer, chemical reactions, and related phenomena by solving mathematical equations that govern these processes using a numerical algorithm on a computer. Many approaches exist for the modelling the motion of two-phase mixtures (*e.g.* solid-liquid), where one phase is dispersed in the other. They can be divided into Eulerian-Lagrangian and Eulerian-Eulerian approaches. In the former approach, the disperse phase is treated in terms of individual particles for which the equations of motion are solved. Solid-liquid flow simulations based on this approach were reported *e.g.* by *Derksen* [1], *Decker* and *Sommerfeld* [2], and *Barrue et al.* [3]. In the Eulerian-Eulerian approach, the two phases are considered to be interpenetrating continua. This approach was used *e.g.* in the papers [4—8], where single- and multiple-impeller stirred tanks were investigated. In majority of these papers, diluted suspensions were studied, well below 1 vol. %, though it is well known that industrial applications often involve higher particle concentrations. Only few papers dealt with CFD modelling of moderately or highly concentrated suspensions. For example, *Barrue et al.* [9] performed the Eulerian-Eulerian simulations of dense suspension with a concentration of 26 vol. % and the "black box method" was used for impeller modelling that requires experimental velocity data at boundary conditions. Fully predictive simulations of

*Presented at the 32nd International Conference of the Slovak Society of Chemical Engineering, Tatranské Matliare, 23—27 May 2005.

**The author to whom the correspondence should be addressed.

dense solid-liquid systems, namely with particle average concentrations in the range of 10 vol. % have been attempted in the papers by *Špidla et al.* [10] and *Micale et al.* [11]. In these works, the multi-fluid approach with a homogeneous treatment of the turbulence was used in conjunction with the Sliding Mesh or Multiple Reference Frames (MRF) algorithms. Good agreement with experimental observation of the particle suspension height was obtained. The momentum exchange *via* interphase drag terms was described by Schiller—Naumann correlation [12], but CFD simulations did not verify the particle concentration distribution within the particle-filled layer.

The particle-filled layer has been commonly observed in the past, and was first discussed by *Musil* [13]. The contributions [10, 11, 14—20] describe the effect of the particle size and concentration, impeller speed, impeller off-bottom clearance, stirrer and vessel size, and physical properties of the system on this phenomenon. Several references are indirect and focused on the study of various suspension system parameters, *e.g.* on the complete suspension conditions. Nevertheless, a review of the particle suspension layer can be found in the above-mentioned works [10, 11]. It should be noted that the particle suspension layer might occur also in three-phase (liquid-gas-solid) systems [18].

Only in the work of *Buurman et al.* [14], there is a note about a relatively homogeneous concentration distribution within the highly concentrated particle-filled layer. The significance of radial concentration gradients within the particle-filled layer has never been analyzed in detail. In literature (not only that interested in the layer of slurry), it is generally considered that the radial concentration gradients are negligible [21—23]. However, this assumption cannot be generalized [24].

The present work is aimed at the exploration of the fully predictive CFD simulation of moderately concentrated suspension with average particle concentration of 5 vol. %. Geometrical vessel configuration and experimental conditions were chosen in order to obtain the particle suspension layer in a stirred vessel. Furthermore, experimental assessment of solid particle distribution within the particle layer was performed by means of a conductivity probe. All experiments were carried out in a pilot-plant stirred tank ($D = 1$ m), and at a state of complete suspension, when no particle remains at the vessel bottom [25]. It should be noted that the present work complements previously published experimental results [20], where the solid distribution for the same experimental conditions was determined in three different planes (baffle plane, 30° and 60° from the baffle plane). In this work, additional solid particle distribution for the midway plane between the vessel baffles (45° from the baffle plane) was determined and the experimental results were compared with simulations.

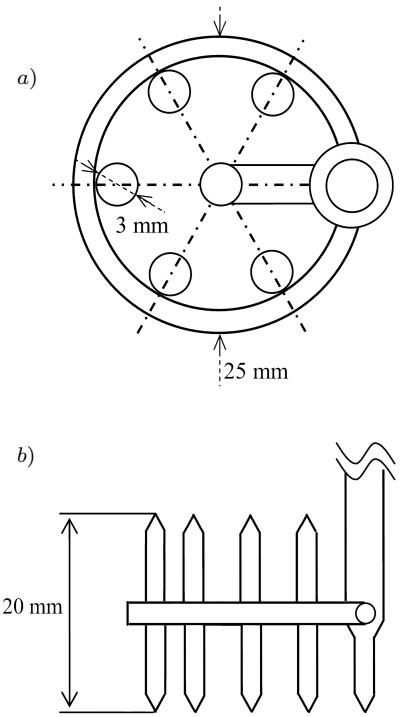

Fig. 1. Conductivity probe.

EXPERIMENTAL

Conductivity measurement was used for determination of the local solid particle distribution. Here, only basic principles and descriptions of conductivity measurement are presented for the sake of brevity, and the reader is encouraged to read the work [20] for further information.

A two-electrode conductivity probe measured the local concentrations of the solid particles (Fig. 1). Volume of the measured space was 6.3 cm^3, compared with the volume of the whole experimental vessel of 7.85×10^5 cm^3. In this case, the influence of the intrusive probe on the suspension process could be considered negligible.

Schematic diagram of the experimental apparatus is shown in Fig. 2. It consisted of a flat-bottomed, cylindrical, transparent Plexiglass, pilot-plant stirred vessel with a diameter $D = 1$ m equipped with four standard baffles, width of baffles was $b = 0.1\ D$. The height of filling, H, in the vessel was equal to the vessel diameter, $H = D$. An optoelectronic disc system coupled with a digital counter was used for measuring the impeller speed. The accuracy of the impeller speed adjustment was $\pm$ 1 min^{-1}.

Temperature calibration of the probe was used for elimination of effects of the temperature-conductivity changes. The linear calibration was determined in a thermostat for a temperature range of 20—30 ℃, at which the experiments were done.

The following relationship of a concentration cal-

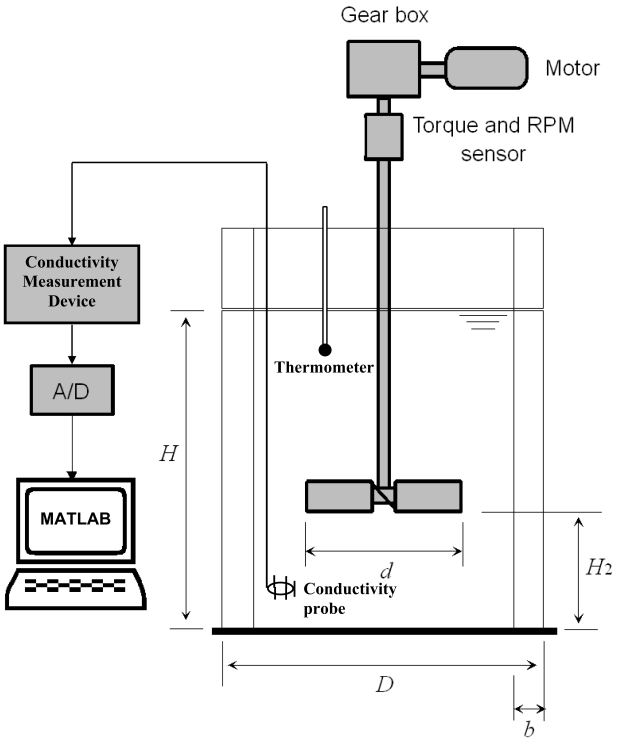

Fig. 2. Experimental set-up with geometrical parameters of the stirred vessel.

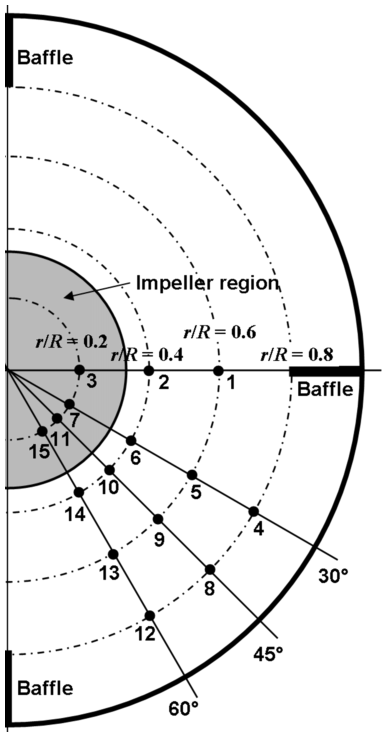

Fig. 3. Location of the measuring points.

ibration was used for calculation of volumetric solid particles concentration

$$\frac{\gamma_\mathrm{s}}{\gamma_\mathrm{f}} = 1 - K_\mathrm{c} c_\mathrm{V} \qquad (1)$$

where K_c is the concentration calibration constant, c_V the local particle concentration, γ_s the conductivity of solid-liquid suspension, and γ_f is the conductivity of the liquid only.

The concentration calibration was performed in a fluidized-bed column, where the probe measured the conductivity γ_s in a uniform suspension layer of a known concentration. The volumetric concentration measured in the settled particle bed was in the range of 0.60—0.63.

Locations of the measuring probe in a horizontal level are shown in Fig. 3. Assuming that the flow inside the vertical quadrants of the vessel was symmetrical, only one quadrant of the vessel volume was investigated, *i.e.* in four vertical planes – the baffle plane, and then at 30°, 45°, and 60° from the baffle plane. Only the results for 45° from the baffle plane are presented here. The solids concentrations were measured in nine horizontal levels with vertical distances from the vessel bottom from 10 cm to 90 cm, with a step of 10 cm. Total number of measuring points was 119. It was not possible to measure in the region under the impeller and at certain points at the height of 90 cm from the vessel bottom. Accuracy of the manual probe adjustment was ± 0.2 cm in the axial and radial directions, and ± 1° in the tangential direction. The impeller rotated in a clockwise direction.

A suspension of classified ballotini in tap water was used as a model suspension at the average concentration $c_{\mathrm{V\,avg}} = 5$ vol. %, corresponding to 11.6 mass %. The mean particle diameter was $d_\mathrm{p} = 0.35$ mm and the particle density was $\rho_\mathrm{p} = 2500$ kg m^{-3}. A flat six-pitched-blade impeller (pitch angle 45°, blade width $w = 0.2d$) was used in the experiments. The vessel-to-impeller diameter ratio was $D/d = 3$ and the impeller off-bottom clearance was $H_2 = d$. For these experimental conditions, the just-suspended agitation speed n_js determined visually was 225 min^{-1}, and it was used in all the experiments.

The iso-concentration contours and the local concentration standard deviations for the vertical plane midway between two baffles (*i.e.* 45° from the baffle plane) are shown in Fig. 4. The experimental axial concentration profiles are presented together with the CFD simulation results in Fig. 7. The experimental results for the other investigated planes (baffle plane and then 30° and 60° from the baffle plane) can be found elsewhere [20]. Dependences are depicted in a form of normalized concentrations $c_\mathrm{V}/c_{\mathrm{V\,avg}}$, and normalized standard deviations $c_{\mathrm{V\,std}}/c_{\mathrm{V\,avg}}$.

These dependences clearly indicate the existence of a particle layer the height of which fluctuated approximately in the range of $h/H \approx 0.65$—0.85 (Figs. 4*a*, *b*). In this region, the normalized concentration devia-

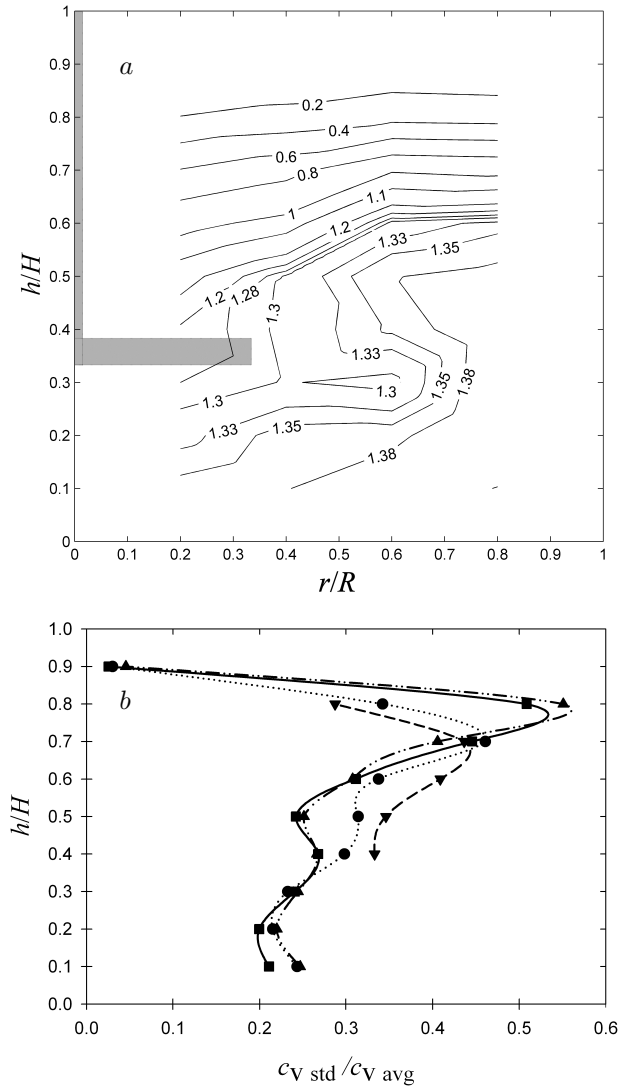

Fig. 4. Normalized particles concentration map $c_V/c_{V\,avg}$ (*a*) and their standard deviations $c_{V\,std}/c_{V\,avg}$ (*b*); midway plane, $c_{V\,avg} = 5$ vol. %, $n_{js} = 225$ min^{-1}. Legend for *b*): $r/R = 0.8$ – dashed-dotted-dotted line with triangles up, $r/R = 0.6$ – solid line with squares, $r/R = 0.4$ – dotted line with circles, $r/R = 0.2$ – dashed line with triangles down.

tions reached their maximum (Fig. 4*b*). The interface between the clear-liquid and the suspension layer was considerably unstable, as a result of turbulent flow.

On the contrary, the concentration fluctuations were smaller between the vessel bottom and the height $h/H \approx 0.5$. In this region, the "fully developed" suspension layer was observed, and the normalized concentration deviations were in the range of $c_{V\,std}/c_{V\,avg} \approx 0.2$—0.3. It may be inferred that a well-ordered flow pattern was formed within the particle layer and as already referred [11], a "compression action" was exerted on the fluid flow pattern.

The local concentration values, c_V, were low in the region above the impeller ($r/R = 0.2$). A radial concentration profile was found in the range of dimensionless radial coordinate $r/R = 0.2$—0.8, where the local concentrations decrease from the vessel wall to the vessel axis. Height of the interface between the clear-liquid layer and the suspension layer was lower in the region above the impeller and was not well recognized. Although the values of $c_{V\,std}/c_{V\,avg}$ for $r/R = 0.2$ reached maximum at the interface, they were lower than the maxima attained in the positions $r/R = 0.4$; 0.6; and 0.8.

CFD SIMULATIONS

For all CFD simulations, the Eulerian-Eulerian multiphase model implemented in the commercial code Fluent 6.2 was used. With this approach, the continuity and the momentum equations are solved for each phase and therefore, the determination of separate flow field solutions is allowed. The simulations adopted here are very similar to those in the works [7, 8, 10, 11], but they were performed in a completely different vessel and experimental configuration.

The continuity and momentum equations for a generic phase q, as reported *e.g.* in [26], are

$$\frac{\partial}{\partial t}(\alpha_q \rho_q) + \nabla(\alpha_q \rho_q \boldsymbol{v}_q) = 0 \qquad (2)$$

$$\frac{\partial}{\partial t}(\alpha_q \rho_q \boldsymbol{v}_q) + \nabla(\alpha_q \rho_q \boldsymbol{v}_q \boldsymbol{v}_q = -\alpha_q \nabla p + \\ + \nabla \bar{\bar{\tau}}_q + \boldsymbol{R}_{pq} + \alpha_q \rho_q (\boldsymbol{F}_g + \boldsymbol{F}_{lift,q} + \boldsymbol{F}_{vm,q}) \qquad (3)$$

The lift force $\boldsymbol{F}_{lift,q}$ and the virtual mass force $\boldsymbol{F}_{vm,q}$ have been neglected in the calculations, because they give a minor contribution to the solution with respect to the other terms [6]. The interphase momentum transfer term, $\boldsymbol{R}_{pq}$, is modelled *via* the drag coefficient C_D as follows

$$\boldsymbol{R}_{sl} = \frac{3}{4}\frac{\alpha_s \rho_s}{d_p} C_D \left|\boldsymbol{v}_s - \boldsymbol{v}_l\right| (\boldsymbol{v}_s - \boldsymbol{v}_l) \qquad (4)$$

The value of C_D depends on the particle Reynolds number

$$Re_p = \frac{\rho_l \left|\boldsymbol{v}_s - \boldsymbol{v}_l\right| d_p}{\eta_l} \qquad (5)$$

The correlation for the drag coefficient calculation proposed by *Schiller* and *Naumann* [12], corresponding to a particle falling in a stagnant fluid, is implemented as a default in the Fluent 6.2.

$$C_{D,still} = \frac{24}{Re_p}(1 + 0.15 \times Re_p^{0.687}) \qquad (6)$$

This model is based on relating C_D to Re_p and consequently it does not take the free stream turbulence of the continuous phase into account. *Pinelli et al.* [27] and *Brucato et al.* [28] have proposed a correlation where a correction factor taking the turbulence

of the carrier phase into account is used, eqns (*7*) and (*8*), respectively.

$$C_{\mathrm{D,turb,1}} = C_{\mathrm{D,still}} \left\{ 0.4 \left[\tanh\left(16 \frac{\lambda}{d_{\mathrm{p}}} - 1 \right) \right] + 0.6 \right\}^{-2} \quad (7)$$

$$C_{\mathrm{D,turb,2}} = C_{\mathrm{D,still}} \left[1 + 8.76 \times 10^{-4} \left(\frac{d_{\mathrm{p}}}{\lambda} \right)^3 \right] \quad (8)$$

Here, $C_{\mathrm{D,still}}$ refers to the value in a quiescent fluid and λ is the Kolmogoroff length scale.

For the turbulent multiphase flow, a standard k-ε turbulence model was used. In this study, the simplest k-ε turbulence model was assumed, referred to as the "Mixture Model", where only a couple of k and ε equations are solved and the physical properties of the mixture are adopted. The two phases are assumed to share the same k and ε values and therefore the interphase turbulence transfer is not considered. The relevant equations of the mentioned turbulence model are not reported here for the sake of brevity and they can be found *e.g.* in works [5, 11, 26].

In order to perform fully predictive simulations of the baffled stirred vessel, the Eulerian-Eulerian multiphase model was coupled with the Multiple Reference Frame (MRF) algorithm. The MRF algorithm assumes that the flow field is steady, with the rotor-stator or impeller-baffle effects being accounted for by suitable coupling. This algorithm can be acceptable in all cases for which the rotor-stator interactions are weak. In the presently investigated case, where the vessel-to-impeller diameter ratio $D/d = 3$ was used, the rotor-stator interactions are weak. Moreover, in contrast to the Sliding Mesh algorithm, the MRF algorithm is not so computationally expensive.

The computational grid adopted in the MRF algorithm is shown in Fig. 5. Thanks to symmetry, only half of the vessel was simulated. Structured grid composed of 595282 hexahedral cells (110 × 55 × 102 along the axial, radial, and tangential coordinates) was created in GAMBIT 2.2 pre-processor. Dense computational grid was used because of the pilot-scale vessel dimensions. The rotor-stator interface location was set in the middle between the impeller tip and the edge of the baffles ($r = 0.283$ m) in the radial direction and between $h = 0.295$ m and $h = 0.432$ m in the axial direction. As shown in Fig. 5, the cell spacing was made smaller in the impeller region where the largest gradients of flow quantities are expected.

The initial conditions were: *a*) liquid at rest and *b*) the solid particles uniformly distributed in the whole vessel volume. The second-order upwind discretization scheme was used for the momentum equations, turbulence kinetic energy (k), and turbulence dissipation rate (ε). The QUICK discretization scheme was used for the volume fraction. All the simulations were performed in double precision and a User-Defined Function (UDF) [29] was used for fixing the total volume

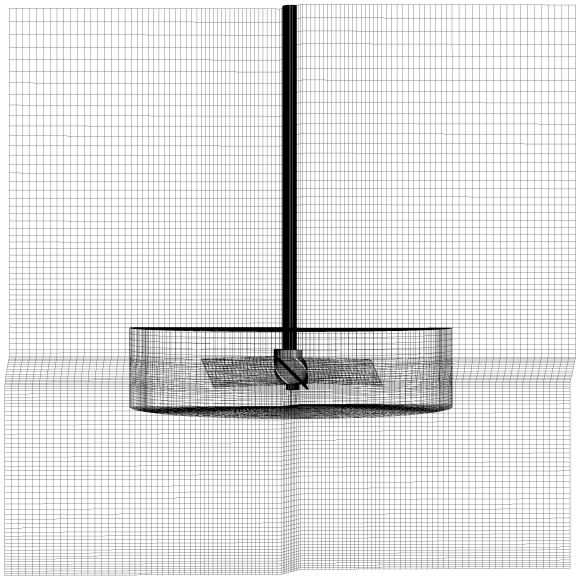

Fig. 5. Structured computational grid with PBT.

fraction in the vessel. A total number of 20000 iterations was found to be sufficient to achieve a fully converged solution.

To improve the convergence behaviour, the flow for only one phase was firstly computed (by deselecting the volume fraction equations). Once the initial solution for the primary phase was obtained, the volume fraction equations were turned back on and the calculation continued with all phases. Moreover, the packing limit of the volume fraction was set to a value of 0.4, to avoid complete settling of the particles at the beginning of the calculation with all phases. The volume fraction was then set back on the default value 0.6. Finally, low under-relaxation factors were used to increase the convergence behaviour.

RESULTS AND DISCUSSION

As referred in the works [5, 7, 8], the drag coefficient C_{D} is critically important parameter for obtaining correct predictions of the solid distribution. Therefore, three different values of C_{D} were used in our simulations. The first was $C_{\mathrm{D,still}} = 2.89$, calculated from the Schiller—Naumann correlation, eqn (*6*), where the free stream turbulence is not taken into account. The other values, $C_{\mathrm{D,turb,1}} = 4.02$ and $C_{\mathrm{D,turb,2}} = 4.92$, were calculated from the Pinelli and Brucato correlations, eqns (*7*) and (*8*), respectively, where the stirred turbulent fluid is taken into account. The average Kolmogoroff length scale λ was calculated from the impeller power input, which was experimentally determined from torque measurements. These manually calculated values of C_{D} were then introduced to the simulations *via* UDF [29].

Comparison of experimental data with different C_{D} correlations in the midway plane at $r/R = 0.8$ (posi-

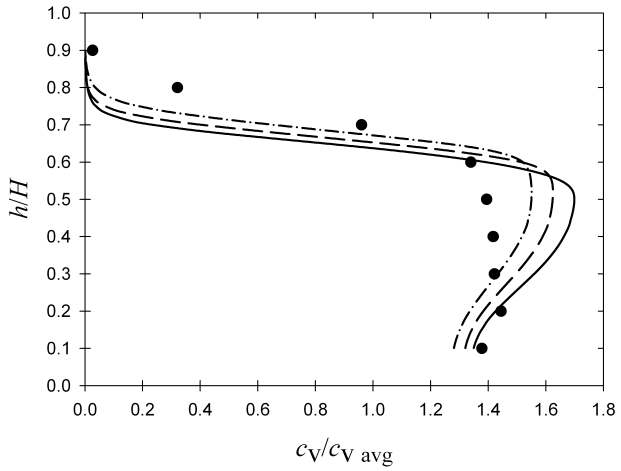

Fig. 6. Comparison of experimental data with CFD simulations using three different drag coefficients; midway plane, $r/R = 0.8$, $c_{V\,avg} = 5$ vol. %, $n_{js} = 225$ min^{-1} (experiment – circles; Schiller—Naumann – solid line; Pinelli – dashed line; Brucato – dotted-dashed line).

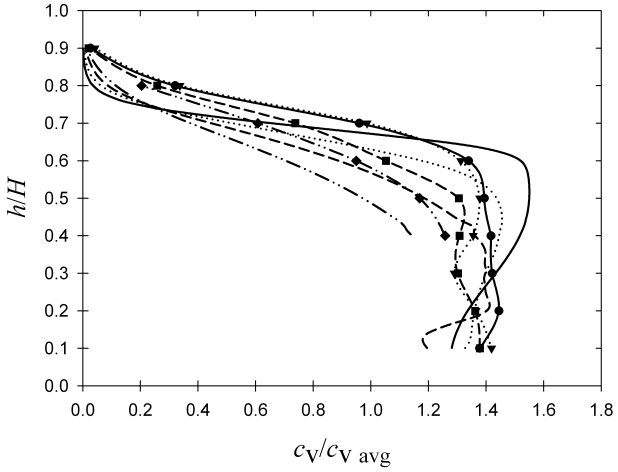

Fig. 7. Comparison of experimental data for different ratios r/R (0.8 – circles; 0.6 – triangles; 0.4 – squares; 0.2 – diamonds) with CFD simulations ($C_{D,turb,2} = 4.92$); midway plane, $c_{V\,avg} = 5$ vol. %, $n_{js} = 225$ min^{-1} (0.8 – solid line; 0.6 – dotted line; 0.4 – dashed line; 0.2 – dotted-dotted-dashed line).

tion 8 in Fig. 3) is shown in Fig. 6. This figure shows the normalized axial concentration profile $c_V/c_{V\,avg}$ and it is clear that significant differences were obtained with different values of C_D. As it can be expected, the lowest cloud height was obtained, when the Schiller—Naumann correlation was used. With this correlation, the highest local concentrations were determined roughly in the height of approx. $h/H \approx 0.5$, where the largest differences between the experimental data and simulations were found. In this region, the calculated local concentrations are by about 20 % higher than the experimental data.

The best fit of experimental data was obtained for C_D calculation according to the Brucato correlation and therefore it was used for further comparison of experimental and computed data (Fig. 7). The cloud height was higher than in the cases of $C_{D,still} = 2.89$ and $C_{D,turb,1} = 4.02$. In addition, the calculated local concentrations in the height of approx. $h/H \approx 0.5$ are closer to experimental values. It could be concluded that the prediction of the cloud height location was good because the results are about 5 cm apart from the experiment. On the other hand, the interface between the suspension layer and the particle-free layer was sharper in the CFD simulations than in the experiments. Moreover, the experimental axial concentration profile was much more homogeneous within the "fully-developed" particle-filled layer.

Comparison of experimental data with simulation using the $C_{D,turb,2} = 4.92$ is shown in Fig. 7 for all investigated radial positions. The experimental concentration profiles are more homogeneous within the "fully-developed" particle-filled layer than in the simulations. Calculated concentration gradient in a radial direction is higher than the experimental one, and the cloud height interface is again sharper in the simulations. As it can be expected, with further increase of the value of C_D, the simulated curves will be closer to the experimental results, at least at the interface between the particle-filled layer and the particle-free layer. It should be noted that eqns (*7*) and (*8*) were determined for dilute suspensions and in completely different vessel configurations. Moreover, it is worth mentioning that the drag coefficient was uniform throughout the entire vessel and it should desirably take into account a distribution of the local particle drag coefficients over the volume of stirred vessel. The average value of the rate of energy dissipation ε calculated from the experimental impeller power input, and used for the calculation of the Kolmogoroff length scale λ, does not correspond to the local values of this quantity. The local values of the C_D can change over the vessel volume within an order of magnitude. This fact has crucial effect on obtaining more accurate CFD results, but correct prediction of local turbulent dissipation is also required, which is not always obtained [11]. Furthermore, no extra terms describing *e.g.* the particle—particle interactions were added into the momentum equations, and only the steady-state simulations were performed.

Calculated concentration maps for all investigated drag coefficients are summarized in Fig. 8. In all cases, the lowest concentrations were determined in the region above the impeller. With increasing the C_D value, concentration gradient in the radial direction decreases and the particle distribution in the "fully-developed" particle layer becomes more homogeneous.

Finally, it can be concluded that a good agreement of simulations with experimental data was obtained, when the location of cloud height in the stirred vessel was studied. The use of higher value of the drag coefficient is recommended and the best results were

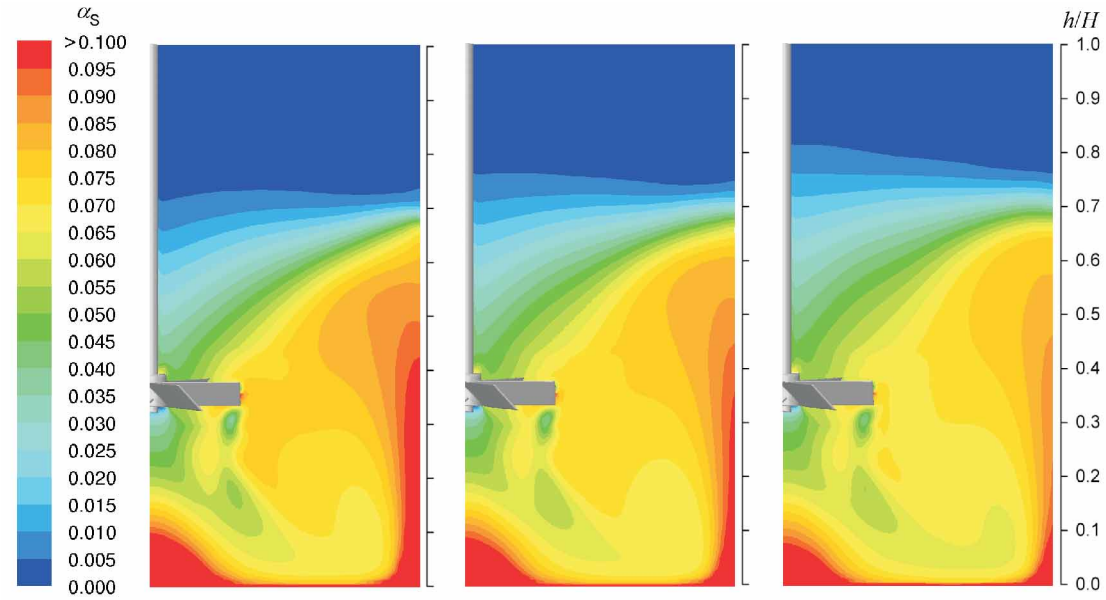

Fig. 8. CFD volume fraction maps: *a*) $C_{D,still} = 2.89$, *b*) $C_{D,turb,1} = 4.02$, *c*) $C_{D,turb,2} = 4.92$.

obtained with Brucato correlation. On the other hand, the concentration distribution within the particle layer is more homogeneous and the radial gradients in the experiments are smaller than the predicted ones.

Acknowledgements. The authors are grateful to Dr. André Bakker from Fluent Inc. in Lebanon (USA) for his valuable advice and comments. The Grant No. 104/03/H141 of the Czech Grant Agency and the Project No. MSM 6046137306 of the Czech Ministry of Education supported this work.

SYMBOLS

b	baffle width	m
C_D	particle drag coefficient	
$C_{D,still}$	particle drag coefficient calculated from eqn (*6*)	
$C_{D,turb,1}$	particle drag coefficient calculated from eqn (*7*)	
$C_{D,turb,2}$	particle drag coefficient calculated from eqn (*8*)	
c_V	local solids volume concentration	vol. %
$c_{V\,avg}$	average solids volume concentration	vol. %
$c_{V\,std}$	standard deviation of the local solids volume concentration	vol. %
D	vessel diameter	m
d	impeller diameter	m
d_p	particle diameter	m
F_g	gravitational force	N
F_{lift}	lift force	N
F_{vm}	virtual mass force	N
H	filling height	m
H_2	impeller off-bottom clearance	m
h	actual position of the measuring point in axial direction	m
K_c	concentration calibration constant in eqn (*1*)	
k	turbulence kinetic energy	$m^2\ s^{-2}$
n_{js}	just-suspended agitation speed	s^{-1}
p	pressure	Pa
R	vessel radius	m
R_{sl}	interphase momentum transfer term (solid-liquid)	$kg\ m^{-2}\ s^{-2}$
Re_p	particle Reynolds number	
r	actual position of the measuring point in a radial direction	m
V	vessel volume	m^3
v	velocity	$m\ s^{-1}$
w	blade width	m

Greek Letters

α	volumetric fraction	
ε	turbulence dissipation	$m^2\ s^{-3}$
γ_f	relative electric conductivity of the liquid	$S\ m^{-1}$
γ_s	relative electric conductivity of the suspension	$S\ m^{-1}$
η	dynamic viscosity	Pa s
λ	Kolmogoroff length scale	m
ρ_l	density of the liquid	$kg\ m^{-3}$
ρ_p	solid density	$kg\ m^{-3}$
τ	stress-strain tensor	Pa

Subscripts

l	referred to the liquid phase
p	referred to the generic phase p
q	referred to the generic phase q
s	referred to the solid phase

REFERENCES

1. Derksen, J. J., *AIChE J. 49*, 2700 (2003).
2. Decker, S. and Sommerfeld, M., *IChemE Symp. Series 140*, 71 (1996).
3. Barrue, H., Xuereb, C., Pitiot, P., Falk, L., and Bertrand, J., *Chem. Eng. Technol. 22*, 511 (1999).
4. Bakker, A., Fasano, J. B., and Myers, K. J., *IChemE Symp. Series 136*, 1 (1994).
5. Micale, G., Montante, G., Grisafi, F., Brucato, A., and Godfrey, J., *Trans. IchemE, Part A, Chem. Eng. Res. Des. 78*, 435 (2000).
6. Ljungqvist, M. and Rasmuson, A., *Trans. IchemE, Part A, Chem. Eng. Res. Des. 79*, 533 (2001).
7. Montante, G., Micale, G., Magelli, F., and Brucato, A., *Trans. IchemE, Part A, Chem. Eng. Res. Des. 79*, 1005 (2001).
8. Montante, G., Rondini, D., Bakker, A., and Magelli, F., *Proceedings of the 15th International Congress CHISA*, Prague, Czech Republic, 2002.
9. Barrue, H., Bertrand, J., Cristiol, B., and Xuereb, C., *J. Chem. Eng. Jpn. 34*, 585 (2001).
10. Špidla, M., Micale, G., Grisafi, F., Brucato, A., and Machoň, V., *Proceedings of the 16th International Congress CHISA*, Prague, Czech Republic, 2004.
11. Micale, G., Grisafi, F., Rizzuti, L., and Brucato, A., *Trans. IchemE, Part A, Chem. Eng. Res. Des. 82*, 1204 (2004).
12. Schiller, L. and Naumann, Z., *Z. Ver. Dtsch. Ing. 1933*, 318.
13. Musil, L., *Chem. Eng. Sci. 39*, 629 (1984).
14. Buurman, C., Resoort, G., and Plaschkes, A., *Chem. Eng. Sci. 41,* 2865 (1986).
15. Shamlou, P. A. and Koutsakos, E., *Chem. Eng. Sci. 44*, 529 (1989).
16. Hicks, M. T., Myers, K. J., and Bakker, A., *Chem. Eng. Commun. 160*, 137 (1997).
17. Bujalski, W., Takenaka, K., Paolini, S., Jahoda, M., Paglianti, A., Takahashi, K., Nienow, A. W., and Etchells, A. W., *Trans. IchemE, Part A, Chem. Eng. Res. Des. 77*, 241 (1999).
18. Takenaka, K., Ciervo, G., Monti, D., Bujalski, W., Etchells, A. W., and Nienow, A. W., *J. Chem. Eng. Jpn. 34*, 606 (2001).
19. Bittorf, K. J. and Kresta, S. M., *Trans. IchemE, Part A, Chem. Eng. Res. Des. 81*, 568 (2003).
20. Špidla, M., Sinevič, V., Jahoda, M., and Machoň, V., *Proceedings of the 31st International Conference SSCHE*, Tatranské Matliare, Slovak Republic, 2004.
21. Barresi, A. and Baldi, G., *Chem. Eng. Sci. 42*, 2949 (1987).
22. Bílek, P. and Rieger, F., *Collect. Czech. Chem. Commun. 55*, 2169 (1990).
23. Yamazaki, H., Tojo, K., and Miyanami, K., *Powder Technol. 48*, 205 (1986).
24. Micheletti, M., Nikiforaki, L., Lee, K. C., and Yianneskis, M., *Ind. Eng. Chem. Res. 42*, 6236 (2003).
25. Zwietering, Th. N., *Chem. Eng. Sci. 8*, 244 (1958).
26. Fluent Incorporated: "Fluent 6.0 Documentation". Lebanon, USA, 2001.
27. Pinelli, D., Montante, G., and Magelli, F., *Chem. Eng. Sci. 59*, 3081 (2004).
28. Brucato, A., Grisafi, F., and Montante, G., *Chem. Eng. Sci. 53*, 3295 (1998).
29. http://www.fluentusers.com/udf_archive/udf_examples/UDF52.htm.